

Non-commutative Index of Measurement-only Entanglement Phase Transition

Zhichen Huang,¹ Chunxiao Du,¹ Yang Zhou,^{1,*} and Zhisong Xiao^{1,2}

¹*School of Physics, Beihang University, Beijing 100191, China*

²*School of Instrument Science and Opto-Electronics Engineering,
Beijing Information Science and Technology University, Beijing 100192, China*

(Dated: March 2, 2026)

Measurement-only models offer an ideal platform for exploring entanglement dynamics in the absence of unitary evolution. Despite extensive numerical evidence for entanglement phase transitions in measurement-only dynamics, the underlying mechanism attributed to non-commutativity among multi-site projective measurements has remained qualitative and coarse-grained. In this work, we identify a quantitative non-commutative index. By applying this index into three representative measurement-only models, we elucidate the role of non-commutativity in measurement-only dynamics: the emergence of a volume-law phase is governed by the non-commutative structure of the measurement ensemble, while the transition point is quantitatively determined by the amount of critical non-commutativity. More strikingly, the critical non-commutativity exhibits a universal linear scaling with the measurement range, independent of the microscopic details of the measurement ensembles. Our findings deepen the understanding of the fundamental mechanism behind the measurement-only entanglement phase transition.

I. INTRODUCTION

Entanglement [1–3] is not only a fundamental feature of quantum many-body systems with no classical counterpart, but also serves as a critical resource for various quantum technologies, such as quantum computation, quantum communication, and quantum metrology [4–7]. As a result, its out-of-equilibrium dynamical behavior in both continuous-time Hamiltonian evolution of conventional condensed matter models and discrete-time evolution of quantum circuit models have attracted more and more interest. The study of entanglement dynamics has led to the discovery of novel entanglement phase transitions (EPTs) [8, 9], characterized by singular changes in the rate of entanglement growth rate or other entanglement properties of steady states. Prominent examples include the many-body localization (MBL) phase transition between a localized phase with logarithmic entanglement growth and a thermalizing phase with algebraic entanglement growth [10–17], as well as the measurement induced phase transition (MIPT) modeled by circuits of random unitary gates interleaved with single-site projective measurements [18–30]. But more intriguingly, measurement alone has the ability to drive a system into different entanglement phases [31, 32]. The circuit schematics for the three dynamics are shown in Fig. 1.

In measurement-only systems, time evolution is driven solely by successive multi-site projective measurements without the application of any unitary gates. Despite the absence of unitary evolution, such systems still display several types of phase transition by adjusting parameters, including a sharp transition between the area law phase to the volume law phase [31], which is similar to the phenomenology of the MIPT model; phase transition between two qualitatively different encoding phases

[32, 33]; topological phase transition is also observed [34–36]. This demonstrates that multi-site joint measurements can both generate and destroy entanglement, in stark contrast to single-site measurements, which act purely as disentangling operations.

For the MBL EPT, it is the competition between disorder and unitary interactions that drives the isolated quantum system to different dynamical entanglement regimes, while the MIPT is generally understood in terms of a competition between the scrambling effects of unitary dynamics and the disentangling effects of single-site measurements. However, the physical origin of entanglement phase transitions in measurement-only systems is fundamentally different from that in unitary Hamiltonian models or unitary-projective circuits. Since no unitary evolution is present, entanglement cannot be attributed to conventional scrambling mechanisms. Instead, it is believed that the key reason for "measurement frustration" that induces scrambling is the non-commutativity among successive multi-site measurement operators. While this picture has been supported by numerical simulations and graph-theoretic arguments, it remains largely qualitative and coarse-grained.

In this work, we systematically investigate a broad class of measurement ensembles and identify a quantitative, ensemble-level indicator that captures the global strength of non-commutativity to predict the location of entanglement phase transitions in measurement-only dynamics. Numerical calculations are performed with the fixed-range factorizable models, the correlated XYZ model, and the mixed-range models. Our results reveal that the stationary entanglement phase in measurement-only dynamics is controlled by two logically distinct factors. First, the emergence of a volume-law entangled steady state is subject to the overall non-commuting structure of the measurement ensemble. Specifically, when the measurement ensemble can be partitioned into two classes such that operators within the same class

* Corresponding author: yangzhou9103@buaa.edu.cn

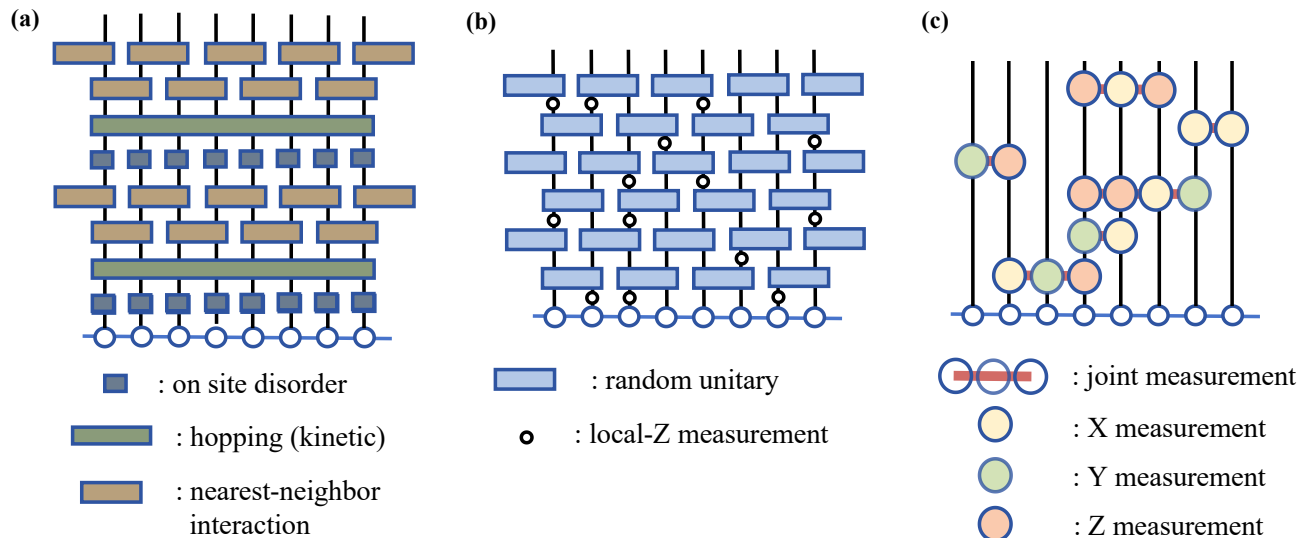


FIG. 1. Circuit schematics for unitary, unitary-projective, and measurement-only dynamics. (a) MBL model represented as a quantum circuit, composed of three qualitatively distinct unitary gates corresponding to the three terms in the MBL Hamiltonian. (b) MIPT circuit in a brick-wall structure of random unitary gates interspersed with local-Z measurements applied at random sites. (c) Measurement-only circuit, consisting solely of joint multi-site measurement operations.

mutually commute, the volume-law phase is prohibited and gives way to a critical phase, which in one dimension exhibits logarithmic scaling with system size. This structural constraint can be described by a bipartite frustration graph as discussed in Ref [31]. Second, the location of the phase transition is quantitatively determined by the amount of non-commutativity, as captured by the index introduced in this work. Notably, we observe that the critical non-commutativity grows linearly with the effective measurement range r . Taken together, these results establish a clear separation between structural constraints and quantitative control parameters in measurement-only entanglement dynamics and provide a unified framework for predicting the onset of entanglement phase transitions.

The remainder of this paper is organized as follows. Sec. II introduces the motivation and formal definition of the non-commutativity index $\mathcal{I}(\mathcal{E})$. In Sec. III, we validate this index through three representative model classes: factorizable models, correlated XYZ model, and mixed-range factorizable models. Finally, Sec. IV summarizes our conclusions and discusses future directions.

II. NON-COMMUTATIVE INDEX OF RANDOM MEASUREMENT ENSEMBLES

In this section, we primarily aim to construct a physical index that quantifies the degree of non-commutativity in a measurement ensemble and governs whether repeated measurements can sustain entanglement growth and drive an entanglement phase transition. In measurement-

only dynamics, entanglement generation arises exclusively from sequences of non-commuting projective measurements. While the ordering of measurements along a single trajectory is stochastic, the overall probability for non-commutation is entirely determined by the measurement ensemble itself. This observation suggests that such an index should be defined at the ensemble level and capture the likelihood that two measurements drawn independently from the ensemble fail to commute.

To render this idea concrete and computationally tractable, we work within the stabilizer formalism [37], which provides an exact and efficient description of measurement-only dynamics involving Pauli operators. According to the Gottesman-Knill theorem [38], quantum states stabilized by Pauli operators can be classically simulated with polynomial computational cost. More importantly for our purposes, the stabilizer framework makes the role of non-commutativity in entanglement dynamics completely explicit. Within this framework, the effect of a projective measurement is completely determined by whether the measured operator commutes or anti-commutes with the existing stabilizer generators. As a result, non-commutativity directly controls the generation, propagation, and suppression of entanglement.

A pure stabilizer state of a one-dimensional qubit chain of length L is specified by a set of L independent, mutually commuting Pauli strings

$$\mathcal{S} = \{g_1, g_2, \dots, g_L\}, \quad (1)$$

which generates the stabilizer group $\mathcal{G} = \langle \mathcal{S} \rangle$. The state

$|\psi\rangle$ stabilized by \mathcal{G} satisfies

$$g|\psi\rangle = +1|\psi\rangle \quad \forall g \in \mathcal{G}. \quad (2)$$

Consider a multi-site projective measurement M represented by a Pauli string operator acting on a stabilizer state $|\psi\rangle$. Two distinct cases arise. If M commutes with all generators in \mathcal{S} , that is $M \in \langle \mathcal{S} \rangle$, and the state is already an eigenstate of the measurement operator, the measurement leaves the stabilizer group unchanged and has no effect on the entanglement dynamics. In contrast, if M anti-commutes with at least one generator in \mathcal{S} , the measurement necessarily modifies the stabilizer group. In this case, one can always choose a generating set such that exactly one generator anti-commutes with M . After the measurement, this generator is replaced by M , while all commuting generators remain unchanged.

It should be pointed out that for Pauli measurements on stabilizer states, the two measurement outcomes occur with equal probability, and the post-measurement stabilizer group differs only by an overall sign that does not affect entanglement properties. Since the entanglement entropy is calculated via the rank of stabilizer tableau, the entanglement dynamics depend solely on whether a measurement operator commutes or anti-commutes with the existing stabilizers, rather than on the specific measurement outcome. Furthermore, owing to the replacement rule described above, the stationary entanglement properties of measurement-only dynamics are independent of the specific choice of initial stabilizers. Instead, entanglement generation and propagation are governed by the frequency with which measurements drawn from the ensemble anti-commute with the current stabilizer generators. This establishes a direct link between entanglement dynamics and the non-commutative structure of the measurement ensemble.

To illustrate this connection explicitly, we simulate the time evolution of the half-chain entanglement entropy along single trajectories, starting from a product state stabilized by $\{Z_1, Z_2, \dots, Z_L\}$, for a factorizable measurement ensemble which will be further illustrated in Sec. III.A. As shown in FIG. 2, when the measurement ensemble is fully commuting ($q = 0$), the entanglement entropy remains strictly zero throughout the evolution, reflecting the absence of any mechanism for entanglement generation. As non-commuting measurements are introduced ($q > 0$), entanglement growth becomes possible: for small q , the entropy fluctuates around a low value and the system relaxes into an area-law steady state. Near the critical point the entropy exhibits slow, approximately logarithmic growth characteristic of a critical phase. For sufficiently large q , the entropy grows linearly at early times before saturating, signaling the emergence of a volume-law steady state. While single-trajectory dynamics does not allow one to unambiguously distinguish between critical and volume-law phases in the stationary regime, these examples clearly demonstrate that non-commutativity is the essential driver of entanglement growth and qualitative changes in the dy-

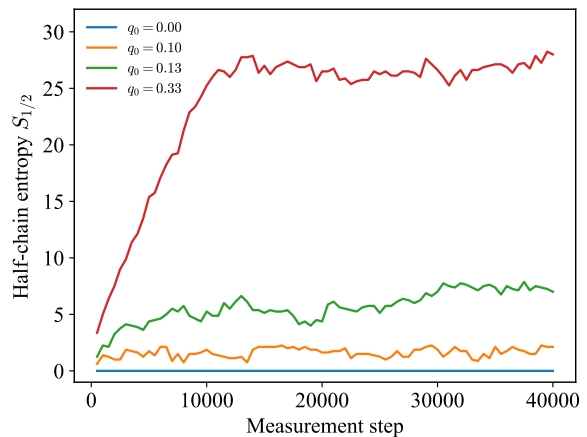


FIG. 2. Time evolution of the half-chain entanglement entropy $S_{1/2}$ along single trajectories for the factorizable measurement ensemble, starting from a pure zero state. Different curves correspond to different values of the probability parameter q , with the constraint $p_x = p_y = q$ and $p_z = 1 - 2q$. The blue curve ($q = 0$) represents the fully commuting case, where the entanglement entropy remains zero at all times and the steady state is area-law. For $q = 0.10$ (orange), non-commuting measurements are present but the system still relaxes to an area-law steady state. At $q = 0.13$ (green), close to the critical point, the entropy exhibits a slow growth characteristic of critical behavior. For $q = 0.33$ (red), the entropy grows linearly at early times and saturates at a value proportional to the system size, indicating a volume-law phase.

namical behavior. These observations allow us to define a non-commutativity index that is independent of initial conditions and measurement outcomes, focusing exclusively on the probability that two measurements drawn independently from the ensemble fail to commute.

We therefore define the non-commutative index of a measurement ensemble \mathcal{E} as:

$$\mathcal{I}(\mathcal{E}) \equiv \sum_{M_1, M_2 \in \mathcal{E}} p(M_1)p(M_2)I(M_1, M_2), \quad (3)$$

where M_1 and M_2 are Pauli operators drawn from measurement ensembles \mathcal{E} with probabilities $p(M_1)$ and $p(M_2)$, respectively. The function

$$I(M_1, M_2) \equiv \begin{cases} 0, & [M_1, M_2] = 0 \\ 1, & \{M_1, M_2\} = 0 \end{cases} \quad (4)$$

serves as an indicator of anti-commutation. By construction, $\mathcal{I}(\mathcal{E})$ represents the probability that two measurements randomly selected from the ensemble do not commute. It is a purely algebraic property of the ensemble and is independent of measurement outcomes, temporal ordering, and the choice of initial state. Importantly, $\mathcal{I}(\mathcal{E})$ does not depend on the entanglement itself, but instead quantifies the intrinsic capacity of the measurement ensemble to generate frustration through non-commuting measurement events. In the following sections, we show

that the critical value of this index governs the entanglement phase transition across a variety of measurement-only models.

III. NON-COMMUTATIVE INDEX FOR PHASE TRANSITION OF MEASUREMENT ONLY DYNAMICS

Having established non-commutativity as the underlying mechanism driving entanglement dynamics in measurement-only models, in this section we examine whether the index defined in Sec. II can serve as an effective indicator for entanglement phase transitions across three representative classes of measurement-only models: the fixed-range factorizable models, the correlated XYZ models, and the mixed-range factorizable models. All numerical calculations are conducted within the stabilizer formalism. The systems are initialized in product states stabilized by $\{Z_1, Z_2, \dots, Z_L\}$ and the entanglement related quantities are calculated through the rank of the corresponding constrained tableau.

A. Fixed-range Factorizable Ensembles

We begin by considering the fixed-range factorizable measurement ensembles proposed in Ref. [31]. Here, our goal is not to revisit their phase structure in detail, but to use them as a controlled setting to verify and quantify the role of operator non-commutativity. In a factorizable ensemble, \mathcal{E} , each measurement operator is a fixed-range Pauli string, acting on r consecutive qubits without identity operators. The Pauli content on different sites is sampled independently and identically, such that the probability of a given Pauli string factorizes into single-site probabilities,

$$P_\alpha = \prod_{j=1}^r p_{\sigma_j}, \quad (\sigma_j = X, Y, Z) \quad (5)$$

with the normalization constraint $p_X + p_Y + p_Z = 1$. As a result, the ensemble is fully specified by two independent parameters, which we choose to be (p_X, p_Y) . Despite their simple construction, factorizable ensembles exhibit rich entanglement dynamics under measurement-only evolution. For sufficiently long interaction range $r \geq 3$, tuning the probability distribution leads to a transition between area-law and volume-law entangled steady states.

For factorizable measurement ensembles with fixed measurement range r , the index, $\mathcal{I}(\mathcal{E})$ can be evaluated either exactly by exhaustive enumeration or efficiently via Monte Carlo sampling. In FIG. 3, we plot $\mathcal{I}(\mathcal{E})$ along two representative directions in parameter space: the symmetric line $p_X = p_Y = q_0$ and $p_Z = 1 - 2q_0$ in FIG. 3(a), and the margin $p_X = q_0, p_Y = 1 - q_0$ and $p_Z = 0$ in FIG. 3(b). It can be seen that, at the

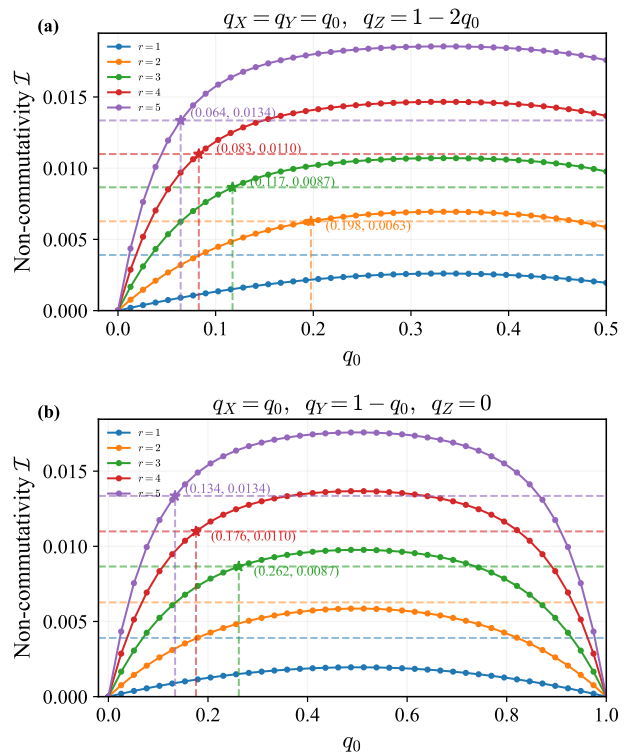


FIG. 3. Non-commutativity index $\mathcal{I}(\mathcal{E})$ of the factorizable measurement ensembles with different measurement ranges r , plotted along two representative directions in probability space. (a) Symmetric line $p_X = p_Y = q_0$ and $p_Z = 1 - 2q_0$. (b) Marginal line $p_X = q_0, p_Y = 1 - q_0$ and $p_Z = 0$. In both cases, $\mathcal{I}(\mathcal{E})$ exhibits a single maximum, located at the maximally symmetric points $p_X = p_Y = p_Z = 1/3$ in (a) and $p_X = p_Y = 1/2, p_Z = 0$ in (b), respectively. The horizontal lines indicate the respectively needed \mathcal{I} for phase transition and the corresponding vertical lines depict the phase transition point.

same probability setting, longer measurement ranges correspond to larger $\mathcal{I}(\mathcal{E})$. Moreover, along both directions, $\mathcal{I}(\mathcal{E})$ exhibits a single maximum. In case (a), the maximal non-commutativity occurs at the fully symmetric point $p_X = p_Y = p_Z = 1/3$, while in case (b) it is reached at $p_X = p_Y = 1/2, p_Z = 0$. These points indicate that ensembles in which non-commuting Pauli operators are most evenly and densely represented have the maximal $\mathcal{I}(\mathcal{E})$.

The transition points of factorizable ensembles can be fitted by Eq. (6) [31]

$$r \simeq \frac{k}{\frac{2}{3} - \delta q^2}, \quad (6)$$

where $k = 1.16$ and δq is defined as

$$\delta q \equiv \sqrt{\left(\frac{1}{3} - p_X\right)^2 + \left(\frac{1}{3} - p_Y\right)^2 + \left(\frac{1}{3} - p_Z\right)^2}. \quad (7)$$

In FIG. 4, we evaluate $\mathcal{I}(\mathcal{E})$ at the transition point along the symmetric line $p_X = p_Y = q_0$ for different interaction ranges r . Remarkably, the critical value \mathcal{I}_c depends

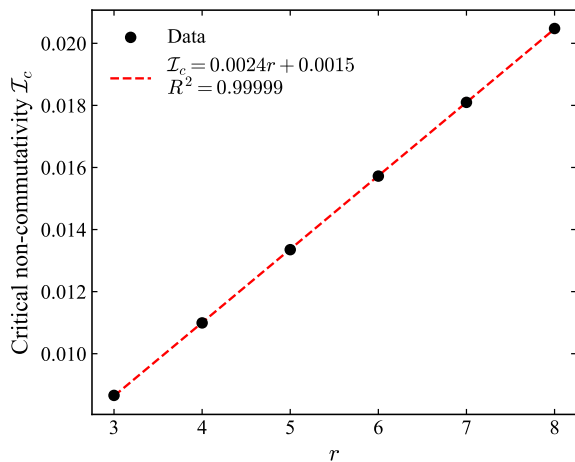


FIG. 4. Critical non-commutativity $\mathcal{I}(\mathcal{E})$ of factorizable measurement ensembles evaluated at the entanglement phase transition along the symmetric line $p_X = p_Y = q_0$ for different interaction ranges r . The transition points $q_{0,critical}$ are determined from the analytical phase boundary given in Eq. (6).

linearly on r ,

$$\mathcal{I}_c = kr + b \quad (8)$$

with $k = 0.0024$, $b = 0.0015$, and coefficient of determination $R^2 = 0.999989$, revealing a robust scaling relation between the interaction range and the amount of ensemble non-commutativity required to sustain a volume-law entangled phase.

While FIG. 4 establishes a clear linear relation between the interaction range r and the critical non-commutativity \mathcal{I}_c along a specific symmetric path in probability space, an important question remains: whether this relation is intrinsic or merely an artifact of the chosen direction. To address this issue, we systematically evaluate \mathcal{I}_c along multiple rays in the measurement-probability simplex. Each ray is defined by an anchor point $(p_X, p_Y, p_Z) \equiv (q_x^{\text{anchor}}, 1 - q_x^{\text{anchor}}, 0)$ on the boundary line $p_Z = 0$. For each anchor, the ray connects the fully symmetric point $(1/3, 1/3, 1/3)$ to the boundary, and the interpolation parameter is fixed such that the distance δq matches the critical value $\delta q_c(r)$ determined from Eq. (6). This construction allows us to probe the phase transition along inequivalent directions while keeping the transition criterion fixed. As demonstrated in FIG. 5, all data collapse onto the same straight line as described by Eq. (8), showing that the critical non-commutativity depends solely on the measurement range r and is insensitive to the direction in probability space along which the transition is approached.

This is quite striking. Different paths toward the phase boundary in measurement probability space typically represent different operator compositions, so it is not a priori obvious that the relationship between critical non-commutativity and the measurement range should

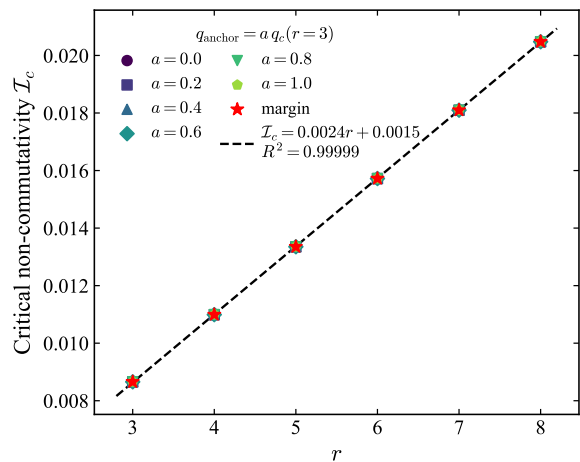


FIG. 5. Critical non-commutativity \mathcal{I}_c for factorizable ensembles extracted along different directions in probability space, including one edge of the parameter space and different 6 center-to-boundary lines of the parameter space. All data collapse onto the same linear $\mathcal{I}_c(r)$, same as Fig.3

be path independent. Different cuts through the probability simplex yield the same $\mathcal{I}_c(r)$, verifying that \mathcal{I}_c serves as a universal control parameter for the entanglement phase transition in factorizable ensembles independent of microscopic details of the measurement ensembles.

Finally, we mark the entanglement phase transition points and the corresponding critical non-commutativity \mathcal{I}_c along the curves for $r = 3$ to $r = 5$ in FIG. 3. The critical non-commutativity \mathcal{I}_c required to induce the phase transition for $r = 1$ and $r = 2$ is also plotted according to Eq. (8). It is indicated that the absence of volume-law phase for $r \leq 2$ is mainly because of the lack of non-commutativity. Notably, for $r = 2$, the curve intersects the critical line at the point $(q_0, \mathcal{I}_c) = (0.198, 0.0063)$ along the symmetric direction $q_X = q_Y = q_0$, $q_Z = 1 - 2q_0$, which suggests the existence of a phase transition. This is consistent with the results of Ref. [31], where a transition from an area-law phase to a critical phase was observed at $\delta q \approx 0.36$, in close agreement with our estimate $\delta q \approx 0.33$. It is suggested that the amount of non-commutativity influences the position of the phase transition, but doesn't determine whether the non-area-law phase is a volume-law phase or a critical phase. We elaborate this point in the next subsection.

B. XYZ Measurement-only Model

We now turn to the XYZ measurement-only models, which provide a natural and nontrivial extension beyond factorizable ensembles. In this model, each measurement operator acts on r consecutive qubits and is chosen randomly from the set of uniform Pauli strings $X^{\otimes r}$, $Y^{\otimes r}$, $Z^{\otimes r}$ with probabilities P_X, P_Y and P_Z . Unlike factoriz-

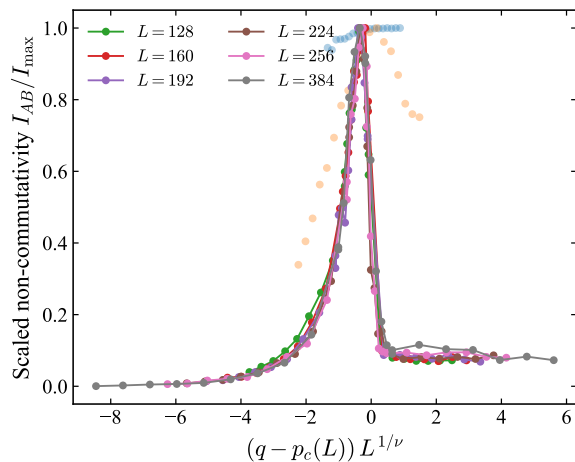


FIG. 6. Finite-size scaling collapse of the mutual information I_{AB} for the XYZ measurement-only model at interaction range $r = 31$ performed with finite-size shifting of the critical point. The data are rescaled according to (10) with the shifted critical point (11) and I_{AB} is further normalized by its peak value for each system size L , such that all curves attain the same maximum. The optimal collapse yields the correlation-length exponent $\nu = 1.3478$ and the thermodynamic critical point $q_c = 0.2522$

able ensembles, the Pauli content within a given measurement operator is fully correlated across its support, rendering the ensemble inherently non-factorizable. A key property of the XYZ models is the strong parity dependence of their entanglement dynamics. when the measurement range r is even, a volume-law entangled steady state is absent. In this case, the system instead exhibits a critical phase characterized by logarithmic scaling of entanglement entropy with system size. By contrast, for odd values of r , a volume-law phase is permitted and the entanglement phase transition from an area-law phase to a volume-law phase is well defined.

In this work, we mainly focus on a systematic examination of how the critical value of ensemble non-commutativity for phase transition depends on the measurement range. Our calculations are performed at $r = 3, 7, 11, \dots, 31$ for odd r and at $r = 2, 4, 6, \dots, 20$ for even r along the symmetric line $P_X = P_Y = q_0, P_Z = 1 - 2q_0$. The entanglement phase transition is characterized by the mutual information I_{AB} [39–41] between two distinct, antipodal region of length $L/8$ of qubit chain with length L in periodic boundary condition. The definition of mutual information is

$$I_{AB} = S_A + S_B - S_{AB}. \quad (9)$$

Finite-size scaling of the mutual information I_{AB} is employed to determine the entanglement phase transition points in the XYZ measurement-only model, which serves as a sensitive probe of long-range correlations. For a continuous transition, the mutual information is expected to

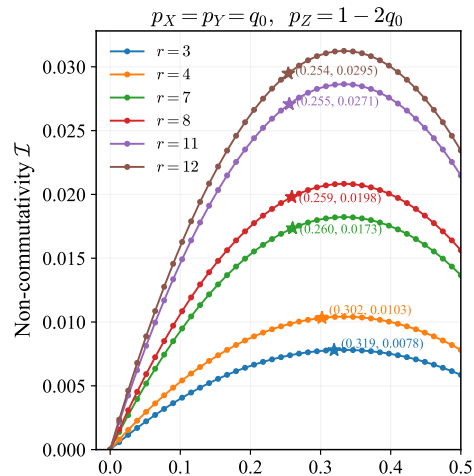


FIG. 7. Non-commutativity index $\mathcal{I}(\mathcal{E})$ of XYZ measurement-only models with measurement range $r = 3, 4, 7, 8, 11, 12$, plotted along symmetric directions in probability space. This figure demonstrates that both even and odd r attain enough Non-commutativity for a phase transition.

obey the scaling form [20]:

$$I_{AB}(L) = F[(q - q_c)L^{1/\nu}], \quad (10)$$

where q denotes the tuning parameter along the symmetric line $P_X = P_Y = q, P_Z = 1 - 2q$. q_c is the critical point in the thermodynamic limit, and ν is the correlation-length exponent.

In finite systems, the apparent transition point exhibits a systematic size dependence. We account for this effect by introducing a finite-size shifted critical point $q_c(L)$, which is assumed to approach its thermodynamic value according to

$$q_c(L) = q_c(L \rightarrow \infty) + AL^{-\nu}, \quad (11)$$

where A is a universal constant for fixed r . In practice, we first perform a preliminary collapse of I_{AB} to obtain initial estimates of q_c and ν . Then, the collapse is refined by tuning the shift parameter A , adjusting the scaling variable $(q - q_c)L^{1/\nu}$ until the optimal data collapse across different system sizes is achieved. This procedure enables a reliable extraction of the thermodynamic transition point q_c for each measurement range r . The corresponding collapsing graph of I_{AB} is shown in FIG. 6. By numerical calculations, we find that the data are well described by the empirical form:

$$\delta q_c(r) \simeq A - \frac{B}{r^\alpha}, \quad (12)$$

with fitting parameters $A = 0.203, B = 1.924$, and $\alpha = 2.219$ for odd r while $A = 0.224, B = 1.375$, and $\alpha = 1.615$ for even r .

Having determined the critical points $q_c(r)$ of the XYZ model numerically, we plot the $\mathcal{I}-q_0$ curves along the

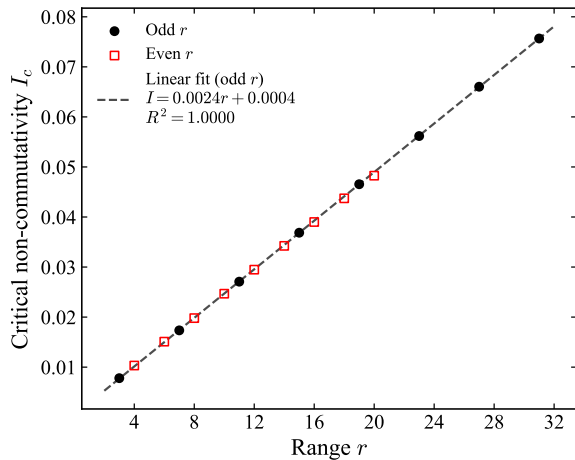


FIG. 8. Critical non-commutativity $\mathcal{I}_c(r)$ as a function of the measurement range r for the XYZ measurement-only model. The black dot and red hollow symbols denote values obtained by evaluating at the numerically determined transition points for odd and even r respectively. The data are well described by a linear fit, $\mathcal{I}_c(r) = kr + b$, with fitting parameters $k = 0.0024$, $b = 0.0004$ and coefficient of determination $R^2 = 0.99$, demonstrating a robust linear scaling of the critical non-commutativity with the measurement range.

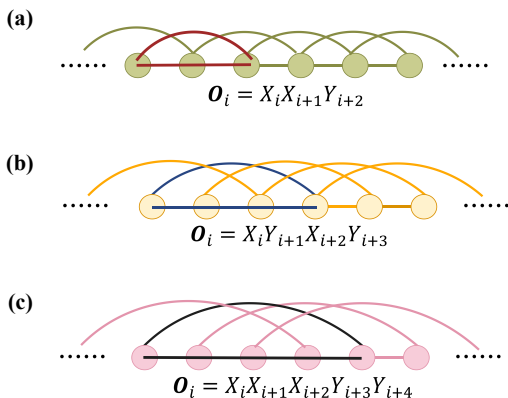


FIG. 9. Non-commutative structure for the cycle-3(a), cycle-4(b), and cycle-5(c) models. The cycle-3 and cycle-5 models are non-bipartite, whereas the cycle-4 model is bipartite. Moreover, the cycle-4 and cycle-5 models do not possess a pairwise non-commuting subset structure, while such a structure exists in the cycle-3 model. The highlighted lines denote the corresponding minimal cycle structure.

symmetric direction $p_X = p_Y = q_0$ and $p_Z = 1 - 2q_0$, and indicate the critical non-commutativity \mathcal{I}_c at the transition point, as shown in FIG. 7. The same trend as FIG. 3 is observed except that for odd r the transition point is from area-law phase to volume-law phase whereas for even r it is from area-law phase to critical phase. Remarkably, as shown in FIG. 8, the resulting $\mathcal{I}_c(r)$ data points for odd r which are represented as black points

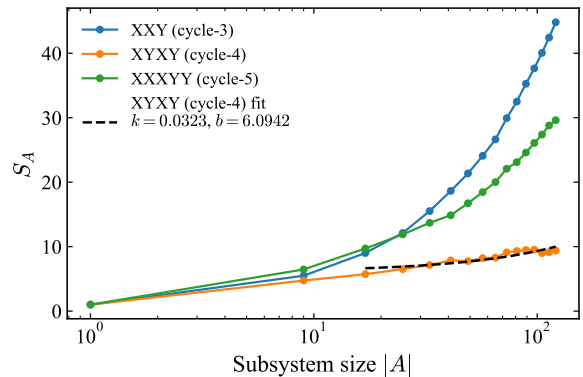


FIG. 10. Bipartite entanglement entropy S_A versus subsystem size $|A|$ for minimal cycle models with different ensemble parity: XXY (cycle-3), $XYXY$ (cycle-4), and $XXXYY$ (cycle-5).

again fall on a straight line, exhibiting the same linear dependence on the measurement range r as observed for factorizable ensembles. This agreement confirms that the linear scaling of the critical non-commutativity is not specific to a particular ensemble construction, but persists across different models. Even more interestingly, the red hollow square points indicating the critical non-commutativity at the transition point for even r also lie around the fitting line though the stationary phase is completely different.

It is argued that the contrasting behaviors of the XYZ models with even r and odd r should be attributed to the different structure of the measurement ensemble: it exhibits a bipartite non-commutativity structure for even r , but becomes non-bipartite for odd r . Here, a “bipartite ensemble” means that the measurement operators can be partitioned into two classes, and that two is the minimal number of classes required such that operators within each class mutually commute. In order to further testify the controlling effect of non-commutativity structures, we construct three minimal measurement ensembles: (1) $\mathcal{E} = \{XXY\}$, (2) $\mathcal{E} = \{XYXY\}$, and (3) $\mathcal{E} = \{XXXYY\}$, referred to as the cycle-3, cycle-4, and cycle-5 models, respectively. Their corresponding non-commutative structure are shown in FIG. 9, where the model label indicates the length of the shortest cycle. The measurement ensembles of the cycle-3 and cycle-5 models are three-bipartite, whereas that of the cycle-4 model is bipartite. Moreover, these three ensembles are distinguished by a finer algebraic structure. Specifically, the cycle-3 model contains a subset of measurement operators with at least three elements that are mutually anti-commuting, while the cycle-5 model does not admit any such subset of pairwise anti-commuting operators, despite being non-bipartite. Equivalently, this reflects the absence of any triangle in its associated frustration graph. We simulate the entanglement dynamics of these ensembles and plot the entanglement entropy as a function of the system size L , as shown in FIG. 10. The results

	Type	Cutoff	Transition q_0
Model1	Uniform	$r = 3, 4, 5, 6$	0.0938
Model2	Uniform	$r = 1, 2, 3, 4, 5, 6$	0.1500
Model3	Exp	$r = 3, 4, 5, 6$	0.1031
Model4	Power	$r = 3, 4, 5, 6$	0.1309

TABLE I. Different models adopted and their transition points along a symmetric direction in parameter space $p_X = p_Y = q_0$, $p_Z = 1 - 2q_0$.

demonstrate that the stationary states exhibit volume-law entanglement for both the cycle-3 and cycle-5 models, whereas the cycle-4 model displays a critical phase with logarithmic scaling. These results imply that a higher degree of separability in non-commutativity structure is required for a stable volume law phase. More importantly, the comparison between the cycle-3 and cycle-5 models shows that the existence of a subset of pairwise anti-commuting operators is not a necessary condition for the emergence of a volume-law phase.

C. Mixed-Range Factorizable Ensembles

So far, our analysis has focused on measurement ensembles characterized by a fixed measurement range r . In this case, the entanglement phase transition is controlled by a critical value of the non-commutativity index $\mathcal{I}_c(r)$, which exhibits a universal linear dependence on r . An important question is whether this picture remains valid when the measurement ensemble contains Pauli strings of multiple ranges. To address this issue, we introduce mixed-range factorizable ensembles, in which the measurement range r is itself a random variable drawn from a prescribed distribution $p(r)$. Physically, the measurement range plays a role analogous to the spatial extent of interactions in many-body systems, and mixed-range ensembles provide a natural setting to test the robustness of the non-commutative index beyond fixed-range models.

In our construction, each measurement operator takes the form

$$O_\alpha \equiv \sigma_i \sigma_{i+1} \dots \sigma_{i+r-1} \quad (13)$$

where the starting site i is chosen uniformly along the chain, the Pauli operators $\sigma_k \in \{X, Y, Z\}$ are sampled independently with probabilities p_X, p_Y, p_Z , and the range r is drawn from a distribution $p(r)$. The probability of selecting a given operator thus reads

$$P_{O_\alpha} = \frac{1}{L} p(r) \prod_{k=i}^{i+r-1} p_{\sigma_k} \quad (14)$$

with $p_X + p_Y + p_Z = 1$. We consider three representative choices of $p(r)$: a uniform distribution over a finite interval, an exponential distribution, and a power-law

distribution. Besides, we choose two different ranges of r for uniform distribution, as summarized in TABLE I. This consideration originates from the fact that for fixed-range factorizable ensembles, $r = 1, 2$ cases do not have a volume-law phase, which implies that they may be qualitatively special. An intuitive expectation would be that the critical point of a mixed-range ensemble can be given by a probabilistic average of the fixed-range transition points,

$$q_c^{naive} = \sum_r p(r) q_c(r). \quad (15)$$

However, direct numerical calculations demonstrate that this naive expectation breaks down.

This failure indicates that the entanglement transition in mixed-range ensembles is not controlled by a simple average of the measurement probabilities, but rather by a more refined quantity associated with non-commutativity. Motivated by the linear relation $\mathcal{I}_c(r) = kr + b$ observed in fixed-range ensembles, we reinterpret the slope

$$k = \frac{\mathcal{I}_c(r) - b}{r} \quad (16)$$

as a characteristic measure of non-commutativity per unit range for a given class of measurement ensembles. For mixed-range ensembles, we therefore define an effective slope

$$k_{eff} = \sum_r p(r) \frac{\mathcal{I}_c(r) - b}{r} \quad (17)$$

and hypothesize that the entanglement phase transition occurs when k_{eff} reaches a universal critical value. The values of k_{eff} extracted at the numerically determined transition points are plotted in FIG. 11. In this model, we obtain the transition points by finite scale collapsing of tripartite mutual information \mathcal{I}_3 [42–44] which is defined by

$$\mathcal{I}_3 = S_A + S_B + S_C - S_{AB} - S_{BC} - S_{CA} + S_{ABC}, \quad (18)$$

where A, B, C are three consecutive interval of length $L/2$. We find that, except for Model 2, all mixed-range ensembles yield values of k_{eff} that are remarkably close to each other. The deviation observed in Model 2 can be traced to the inclusion of short-range measurements with $r = 1, 2$, which are qualitatively distinct: such measurements predominantly destroy entanglement and lack the ability to generate or reorganize long-range correlations. This observation is consistent with the absence of a volume-law phase in fixed-range ensembles with $r \leq 2$.

Taken together, these results demonstrate that the non-commutativity index provides a unified quantitative description of entanglement phase transitions even in measurement ensembles with distributed measurement ranges, provided that measurements capable of generating long-range correlations are sufficiently represented.

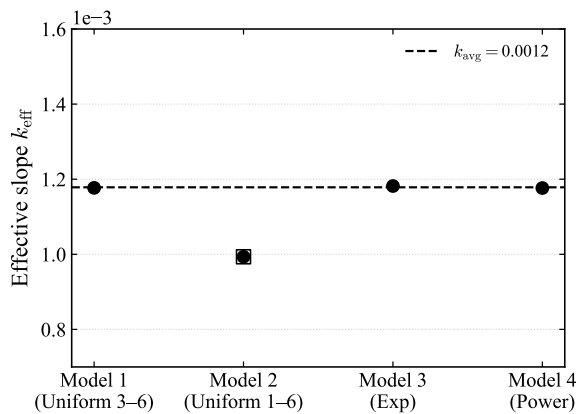


FIG. 11. Effective slope k_{eff} extracted at the entanglement phase transition for different mixed-range factorizable ensembles. Each symbol corresponds to a distinct choice of the range distribution $p(r)$, as summarized in Table I, with k_{eff} defined by the weighted contribution of fixed-range critical non-commutativity. The horizontal dashed line marks the averaged value of k_{eff} of Model 1,3,4. All models except Model 2, which includes short-range measurements with $r = 1, 2$, are close, demonstrating that the entanglement transition in mixed-range ensembles is controlled by the same non-commutativity criterion.

IV. CONCLUSION

In this work, we have systematically investigated the physical mechanism underlying entanglement phase transitions driven only by measurements, with particular emphasis on the role played by non-commutativity among measurement operators. Unlike unitary or hybrid cir-

cuits, where entanglement growth is driven by unitary scrambling processes, measurement-only dynamics admit no intrinsic unitary evolution. The emergence of nontrivial entanglement phases must therefore originate purely from the algebraic structure of the measurement ensemble itself.

Our main result is the identification of a quantitative ensemble-level non-commutative index, $\mathcal{I}(\mathcal{E})$, which captures the global strength of anti-commutation within a measurement ensemble. By employing this index into three representative measurement-only models – fixed-range factorizable ensembles, the fully correlated XYZ model, and mixed-range factorizable ensembles – we unveil the role of non-commutativity in measurement-only dynamics: For higher than bipartite ensembles, when the non-commutative index $\mathcal{I}(\mathcal{E})$ is sufficiently large, the system can be driven into a volume-law phase. The critical non-commutativity \mathcal{I}_c is solely related to the measurement range r and is independent of microscopic details of the measurement probabilities. The linear scaling $\mathcal{I}_c = kr + b$ has been proven universal and effective across different models. However, for bipartite ensembles, the volume-law phase is absent even for sufficiently large $\mathcal{I}(\mathcal{E})$. These findings establish a unified framework for understanding entanglement phase transitions in measurement-only systems.

V. ACKNOWLEDGMENTS

This work was supported by the National Natural Science Foundation of China under Grant No.61975005 and No.12474556, the Beijing Academy of Quantum Information Science under Grants No.Y18G28, and the Fundamental Research Funds for the Central Universities.

-
- [1] A. Einstein, B. Podolsky, and N. Rosen, Can quantum-mechanical description of physical reality be considered complete?, *Phys. Rev.* **47**, 777 (1935).
 - [2] E. Schrödinger, Die gegenwärtige situation in der quantenmechanik, *Naturwissenschaften* **23**, 807–812 (1935).
 - [3] R. Horodecki, P. Horodecki, M. Horodecki, and K. Horodecki, Quantum entanglement, *Rev. Mod. Phys.* **81**, 865 (2009).
 - [4] M. A. Nielsen and I. L. Chuang, *Quantum Computation and Quantum Information*, 1st ed. (Cambridge University Press, 2000).
 - [5] C. H. Bennett, G. Brassard, C. Crépeau, R. Jozsa, A. Peres, and W. K. Wootters, Teleporting an unknown quantum state via dual classical and einstein-podolsky-rosen channels, *Phys. Rev. Lett.* **70**, 1895 (1993).
 - [6] C. H. Bennett, G. Brassard, S. Popescu, B. Schumacher, J. A. Smolin, and W. K. Wootters, Purification of noisy entanglement and faithful teleportation via noisy channels, *Phys. Rev. Lett.* **76**, 722 (1996).
 - [7] E. Chitambar and G. Gour, Quantum resource theories, *Rev. Mod. Phys.* **91**, 025001 (2019).
 - [8] A. Osterloh, L. Amico, G. Falci, and R. Fazio, Scaling of entanglement close to a quantum phase transition, *Nature* **416**, 608 (2002).
 - [9] K. Kawabata, T. Numasawa, and S. Ryu, Entanglement phase transition induced by the non-hermitian skin effect, *Phys. Rev. X* **13**, 021007 (2023).
 - [10] P. W. Anderson *et al.*, Absence of diffusion in certain random lattices, *Physical review* **109**, 1492 (1958).
 - [11] D. A. Abanin, E. Altman, I. Bloch, and M. Serbyn, Colloquium: Many-body localization, thermalization, and entanglement, *Rev. Mod. Phys.* **91**, 021001 (2019).
 - [12] D. M. Basko, I. L. Aleiner, and B. L. Altshuler, Metal-insulator transition in a weakly interacting many-electron system with localized single-particle states, *Annals of Physics* **321**, 1126 (2006).
 - [13] V. Oganesyan and D. A. Huse, Localization of interacting fermions at high temperature, *Phys. Rev. B* **75**, 155111 (2007).
 - [14] A. Pal and D. A. Huse, Many-body localization phase transition, *Phys. Rev. B* **82**, 174411 (2010).

- [15] M. Serbyn, Z. Papić, and D. A. Abanin, Universal slow growth of entanglement in interacting strongly disordered systems, *Phys. Rev. Lett.* **110**, 260601 (2013).
- [16] M. Serbyn, Z. Papić, and D. A. Abanin, Local conservation laws and the structure of the many-body localized states, *Phys. Rev. Lett.* **111**, 127201 (2013).
- [17] R. Nandkishore and D. A. Huse, Many-body localization and thermalization in quantum statistical mechanics, *Annu. Rev. Condens. Matter Phys.* **6**, 15 (2015).
- [18] A. Chan, R. M. Nandkishore, M. Pretko, and G. Smith, Unitary-projective entanglement dynamics, *Phys. Rev. B* **99**, 224307 (2019).
- [19] B. Skinner, J. Ruhman, and A. Nahum, Measurement-induced phase transitions in the dynamics of entanglement, *Phys. Rev. X* **9**, 031009 (2019).
- [20] Y. Li, X. Chen, and M. P. A. Fisher, Measurement-driven entanglement transition in hybrid quantum circuits, *Phys. Rev. B* **100**, 134306 (2019).
- [21] Y. Li, X. Chen, and M. P. A. Fisher, Quantum zeno effect and the many-body entanglement transition, *Phys. Rev. B* **98**, 205136 (2018).
- [22] T. Minato, K. Sugimoto, T. Kuwahara, and K. Saito, Fate of measurement-induced phase transition in long-range interactions, *Phys. Rev. Lett.* **128**, 010603 (2022).
- [23] C.-M. Jian, Y.-Z. You, R. Vasseur, and A. W. W. Ludwig, Measurement-induced criticality in random quantum circuits, *Phys. Rev. B* **101**, 104302 (2020).
- [24] I. Poboiko, I. V. Gornyi, and A. D. Mirlin, Measurement-induced phase transition for free fermions above one dimension, *Phys. Rev. Lett.* **132**, 110403 (2024).
- [25] K. Yokomizo and Y. Ashida, Measurement-induced phase transition in free bosons, *Phys. Rev. B* **111**, 235419 (2025).
- [26] S.-K. Jian, C. Liu, X. Chen, B. Swingle, and P. Zhang, Measurement-induced phase transition in the monitored sachdev-ye-kitaev model, *Phys. Rev. Lett.* **127**, 140601 (2021).
- [27] Q. Tang and W. Zhu, Measurement-induced phase transition: A case study in the nonintegrable model by density-matrix renormalization group calculations, *Phys. Rev. Res.* **2**, 013022 (2020).
- [28] P. Sierant, M. Schirò, M. Lewenstein, and X. Turkeshi, Measurement-induced phase transitions in $(d + 1)$ -dimensional stabilizer circuits, *Phys. Rev. B* **106**, 214316 (2022).
- [29] Y. Bao, S. Choi, and E. Altman, Theory of the phase transition in random unitary circuits with measurements, *Phys. Rev. B* **101**, 104301 (2020).
- [30] Y. L. Gal, X. Turkeshi, and M. Schirò, Volume-to-area law entanglement transition in a non-Hermitian free fermionic chain, *SciPost Phys.* **14**, 138 (2023).
- [31] M. Ippoliti, M. J. Gullans, S. Gopalakrishnan, D. A. Huse, and V. Khemani, Entanglement phase transitions in measurement-only dynamics, *Phys. Rev. X* **11**, 011030 (2021).
- [32] N. Lang and H. P. Büchler, Entanglement transition in the projective transverse field ising model, *Phys. Rev. B* **102**, 094204 (2020).
- [33] Y. Li and M. P. A. Fisher, Decodable hybrid dynamics of open quantum systems with F_2 symmetry, *Phys. Rev. B* **108**, 214302 (2023).
- [34] Y. Kuno and I. Ichinose, Emergence symmetry protected topological phase in spatially tuned measurement-only circuit, arXiv preprint arXiv:2212.13142 (2022).
- [35] A. Lavasani, Y. Alavirad, and M. Barkeshli, Topological order and criticality in $(2 + 1)$ D monitored random quantum circuits, *Phys. Rev. Lett.* **127**, 235701 (2021).
- [36] K. Klocke and M. Buchhold, Topological order and entanglement dynamics in the measurement-only xxx quantum code, *Phys. Rev. B* **106**, 104307 (2022).
- [37] S. Aaronson and D. Gottesman, Improved simulation of stabilizer circuits, *Phys. Rev. A* **70**, 052328 (2004).
- [38] D. Gottesman, Group22: Proceedings of the xxii international colloquium on group theoretical methods in physics (1999).
- [39] C. E. Shannon, A mathematical theory of communication, *The Bell System Technical Journal* **27**, 379 (1948).
- [40] C. Adami and N. J. Cerf, von neumann capacity of noisy quantum channels, *Phys. Rev. A* **56**, 3470 (1997).
- [41] H. Ollivier and W. H. Zurek, Quantum discord: A measure of the quantumness of correlations, *Phys. Rev. Lett.* **88**, 017901 (2001).
- [42] J. A. T. Thomas M. Cover, Entropy, relative entropy, and mutual information, in *Elements of Information Theory* (John Wiley & Sons, Ltd, 2005) Chap. 2, pp. 13–55, <https://onlinelibrary.wiley.com/doi/pdf/10.1002/047174882X.ch2>.
- [43] V. Coffman, J. Kundu, and W. K. Wootters, Distributed entanglement, *Phys. Rev. A* **61**, 052306 (2000).
- [44] P. Hayden, M. Headrick, and A. Maloney, Holographic mutual information is monogamous, *Phys. Rev. D* **87**, 046003 (2013).
- [45] Y. Kuno and I. Ichinose, Emergence symmetry protected topological phase in spatially tuned measurement-only circuit (2022), arXiv:2212.13142 [cond-mat.stat-mech].